

A dynamic carbon flow traceability framework for integrated energy systems

Bowen Zhang ^{a,b}, Baligen Talihati ^{a,b}, Hongtao Fan ^{a,b}, Yaojie Sun ^{a,b,*} , Yu Wang ^{a,b,**}

^a College of Intelligent Robotics and Advanced Manufacturing, Fudan University, 200433, Shanghai, China

^b Shanghai Engineering Research Center for AI in Integrated Energy Systems, Fudan University, 200433, Shanghai, China

ARTICLE INFO

Keywords:
IES
Energy-carbon flow mapping
LCA
Carbon network
Traceability

ABSTRACT

Carbon flow analysis plays a crucial role in understanding carbon emissions in integrated energy systems (IES), serving as the basis for constructing carbon networks. Among existing methods, the carbon factor approach is commonly used to derive carbon flow data. However, those carbon factors are essentially statistical averages, which lead to inaccuracies and a lack of dynamic characteristics. This absence of dynamic features results in ambiguity in the allocation of carbon emissions within IES. To address this issue, this study proposes the concept of energy-carbon flow mapping, integrating carbon emission factors and utilizing network analysis. Specifically, life cycle analysis (LCA) methods are employed to enhance precision, and energy-carbon flow mapping is used to construct a dynamic carbon network. This approach successfully improves the spatiotemporal resolution and traceability of carbon emissions, enabling precise quantification and analysis. In essence, this study presents a framework for determining the traceability of energy-related carbon emissions. A virtual IES14 carbon network model is constructed for an industrial park in Nanjing to demonstrate the feasibility of this method. The results demonstrate that the proposed model and analytical approach are effective and accurate in quantifying the spatiotemporal distribution of carbon emissions. Furthermore, the carbon footprint of energy can be efficiently traced, laying a solid foundation for future discussions on risk profiling and the optimization of low-carbon energy dispatch in IES.

1. Introduction

The global pursuit of carbon peaking and carbon neutrality goals has led to an intensification of research into carbon reduction strategies within energy systems. It is well documented that conventional energy systems are major contributors of CO₂ emissions. Integrated Energy Systems (IES), however, present a promising alternative, by facilitating the integration of renewable energy (RE) and improve overall energy efficiency (Talihati et al., 2024). It is of paramount importance to conduct accurate carbon accounting for assessing and optimizing the potential for carbon reduction in IES. As a result, carbon emission flow (CEF) analysis in IES has become a central focus of contemporary research (Zeng et al., 2020).

The existing methodologies for calculating CEF are grounded in internationally recognized standards, including the ISO, IPCC and PAS frameworks. These frameworks provide the necessary consistency and

methodological rigor for carbon accounting practices.

Two principal traceability techniques are typically employed: the carbon factor method, noted for its simplicity and practicality in static scenarios (Meng et al., 2018; Cheng et al., 2019a), and Life Cycle Assessment (LCA), which assesses carbon flows throughout the life cycle offers a more detailed and comprehensive assessment (Tranberg et al., 2018; Wang et al., 2015; Cheng et al., 2019b). Although LCA is an effective method for comprehensive analysis, its extended temporal scope limits its applicability to real-time energy networks system operations. In order to address these challenges, carbon flow evaluation has been proposed in (Li et al., 2013), demonstrating greater accuracy in power system analysis compared to other sectors.adaptation of CEF methodologies to intricate IES scenarios (Kang et al., 2022). The integration of CEF with grid-side models enables the more accurate quantification of emissions throughout the energy supply process, thereby facilitating greater precision in dynamic carbon flow analysis.

* Corresponding author. Fudan University, Shanghai, 200433, China.

** Corresponding author. Fudan University, Shanghai, 200433, China.

E-mail addresses: yjsun@fudan.edu.cn (Y. Sun), y_wangfdu@fudan.edu.cn (Y. Wang).

Table 1

Comparison of CEF models for IES scenarios.

Ref.	Grid	Gas	Hot	RE	Method	CEC	Spatial	Temporal
Zhang et al. (2022)	✓	✗	✗	✗	MF	✗	✓	✗
Wang et al. (2023), Li et al. (2023), Wang et al. (2022), Yang et al. (2023), Yan et al. (2023)	✓	✗	✗	✗	CF	✗	✗	✗
Wang et al. (2024), Zhang et al. (2022)	✓	✗	✗	✗	CF	✓	✓	✗
Jiang et al. (2018), Cheng et al. (2019), Deng (2019), Yu et al. (2021), Wang et al. (2016)	✓	✓	✓	✗	CF	✗	✗	✗
Zhen et al. (2024)	✓	✓	✓	✓	CF	✓	✓	✗
Wang et al. (2024)	✓	✓	✓	✗	LCA	✗	✓	✗
This work	✓	✓	✓	✓	LCA	✓	✓	✓

Notes: CEC: carbon emissions composition; MF: material flow; CF: carbon factor.

Nevertheless, single source models are inadequate for IES scenarios where energy flows are inherently coupled at multi-energy nodes (Wang et al., 2024; Zhang et al., 2022; Zhang et al., 2022, 2022; Cui et al., 2023). Recent studies Hu et al. (2021), Yang et al. (2023), Zhen et al. (2024) have developed sophisticated CEF models that allocate emissions across energy hubs (EHs), thereby facilitating detailed analyses of energy transfer and conversion processes. Furthermore, the integration of life-cycle perspectives into CEF has enhanced long-term accuracy (Wang et al., 2022, 2023; Li et al., 2023; Yang et al., 2023; Yan et al., 2023), as evidenced by studies Jiang et al. (2018), Cheng et al. (2019), Deng (2019), Yu et al. (2021), Wang et al. (2016). However, the current limitations persist, including fragmented temporal analyses and restricted real-time assessment capabilities.

To address these limitations, future research should focus on unified and dynamic CEF frameworks that integrate multi-energy coupling, life-cycle considerations and real-time system dynamics. Such approaches

are essential to accurately capture the spatiotemporal complexity of carbon flows in IES, and ultimately provide actionable insights to support carbon abatement strategies in modern energy systems.

This study investigates the CEF model within IES scenarios (Table 1) and presents the overall analytical framework, as illustrated in Fig. 1. In order to enhance the traceability of carbon emissions, we propose a dynamic methodology for constructing and analyzing carbon network. This methodology will establish a traceable CEF network model capable of dynamic and precise carbon emission analysis in complex energy scenarios. The principal contributions of this study are summarized as follows:

1. The mapping between energy and carbon flows, along with the analysis of transmission pathway losses, constitutes a core contribution of this study. A network model is characterized the relationship between energy and carbon flows, with a particular focus on

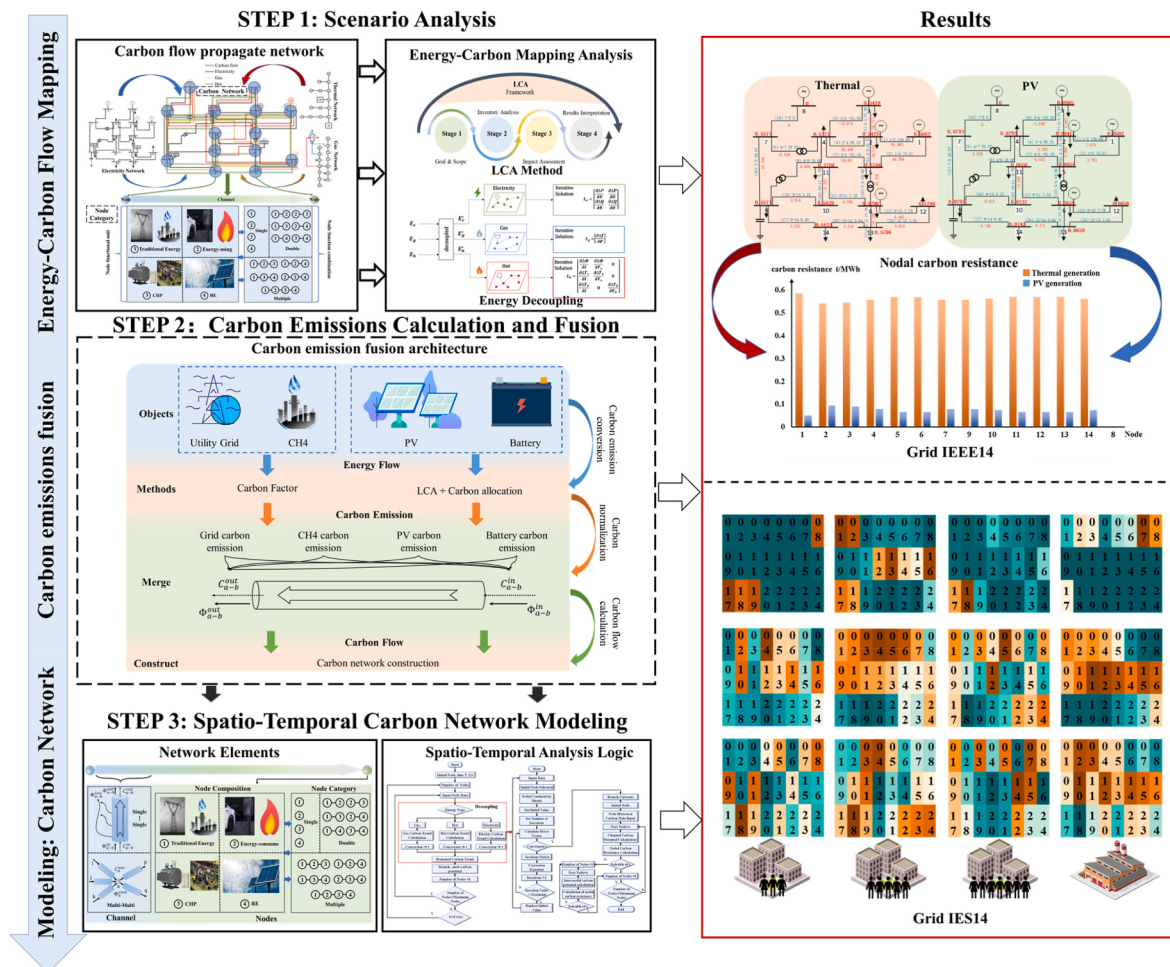


Fig. 1. IES energy-carbon flow mapping analyze framework.

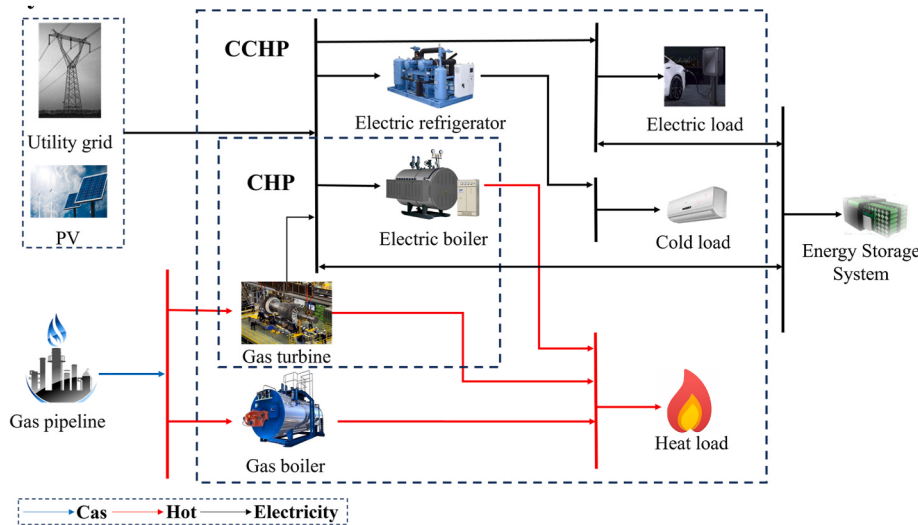


Fig. 2. IES scenario.

- pathway losses based on node considerations. A generalized method for the transformation of energy and carbon is proposed for use with network nodes and transmission pathways. This offers a refined and scalable approach for the construction of CEF model construction.
2. The integration of life-cycle and carbon factor methods represents a significant advancement in the field of environmental science. This study subdivides CEF into historical and current carbon emissions by combining the LCA method with the carbon factor method. The allocation of historical emissions is based on the entire lifecycle of energy production, thereby providing a unified perspective of carbon emissions. This approach improves the precision of CEF accounting by differentiating emissions across a range of energy sources and production processes.
 3. This work provides a spatiotemporal analysis of the carbon emission network. The spatial dimension of the proposed CEF network model is analyzed using directional flow trends, which reveal the potential for carbon transfer and distribution at each node. From a temporal standpoint, the model allows for the characterization of carbon loads at different times, thereby providing insights into the time-varying user demands and emission profiles.
 4. The proposed model enables dynamic carbon traceability within IES. A novel traceability method is proposed, which leverages dynamic analysis and precision tracking to enhance the accuracy and adaptability of carbon emission assessments across varying operational conditions. This method provides a comprehensive and scalable framework for carbon emission analysis in IES.

The remainder of the paper is organized as follows: Section 2 introduces the key metrics and fundamentals for carbon networks in IES. Section 3 develops the IES energy-carbon flow network model using diverse energy network configurations. Section 4 outlines the general procedure of the proposed model. Section 5 validates the feasibility of the model through a case study, including the analysis of key indicators. Section 6 concludes the paper with a summary of findings and implications.

Nomenclature			
CEF	Carbon emission flow	C	CEF, t
LCA	Life cycle analysis	C_{LCA}	CEF in LCA, t
IES	Integrated energy systems	C_{out}	CEF in node, t
IOS	Input-Output approach	$C_{clean\ use}$	CEF of RE in node, t
IPCC	Intergovernmental panel on climate change	C_{loss}	CEF of energy lose, t
EH	Energy hub	ϕ_i	Energy flow in node, MWh
		ϕ_{total}	Energy flow in life cycle, MWh

(continued on next column)

(continued)

CHP	Heat and power unit	m_l	Energy flow in line, MWh
CCHP	Cold heat and power unit	R	Branch carbon resistance, t/MWh
PV	Photovoltaics	V	Nodal carbon potential, t
GB	Gas boiler	E	Electric load, MWh
RE	Renewable energy	G	Gas load, m³
Symbols		Q	Thermal energy load, MJ
ρ	Carbon factor, t/MWh	η	Conversion efficiency
ρ_{his}	Carbon factor in history, t/MWh	ε	Enhanced accuracy of CEF
ρ_{cur}	Carbon factor in current, t/MWh	τ	RE carbon utilization rate
		ξ	Energy carbon utilization rate

2. Key features and fundamentals

The system scenario is illustrated in Fig. 2. The energy supply side comprises the grid, thermal energy network, and green power photovoltaic power generation. The energy demand side includes cooling, heating, and electricity loads. The energy conversion and coupling components include electric boilers, generators, and heat exchangers that enable the transformation among cooling, heating, and electricity.

The integrated energy network scenarios can be analyzed from both carbon emission and economic perspectives. Single-dimensional carbon emission analysis supports simplified and consistent operation planning within IES networks.

2.1. Basic concept

To comprehensively assess carbon sources and their relationship to energy carriers within the network, carbon emissions are analyzed from three perspectives. Carbon emissions are analyzed in three dimensions: the energy side, the transmission side, and the node side, respectively.

On the energy side, carbon emissions are categorized into current and historical carbon emissions based on the time dimension.

$$\rho = \rho_{his} + \rho_{cur} \quad (1)$$

$$\rho_{his} = \frac{C_{LCA}}{\phi_{total}} \quad (2)$$

Where ρ is the unit emission coefficient of energy; ρ_{his} and ρ_{cur} denote the current carbon emission coefficient and the historical carbon emission coefficient. The historical carbon emission factor is determined by its

carbon emission C_{LCA} under the full life cycle analysis with its energy output ϕ_{total} under the full life cycle.

The transmission side analyzes the interrelationship between energy flow and carbon flow, and proposes carbon flow parameters and carbon resistance of the transmission link.

$$C_{line} = R^* \phi_{line} \quad (3)$$

Where C_{line} is the carbon flow in the link, indicating the carbon flow under the current link; R is the link carbon resistance, indicating the carbon emission strength of the current transmission energy flow; ϕ_{line} is the energy flow size of the current link.

$$\epsilon = \frac{C_{his}}{C_{cur} + C_{his}} \quad (4)$$

The carbon emission accuracy improvement factor ϵ is proposed to characterize the carbon emission accuracy improvement under the LCA method.

The node side considers the carbon emission potential of the current node, which is a significant factor in the generation of carbon resistance in the link. Since there are losses in the process of transmission and transformation of energy, the energy utilization rate of the current node is set to evaluate, where the main losses come from the transformation of energy flow and a small portion comes from inter-nodal transmission. Finally, the RE consumption rate of the node is also considered to evaluate the RE consumption of the nodes.

$$C_{out} = V^* \phi_{out} \quad (5)$$

Where C_{out} is the node's carbon flow output, ϕ_{out} is the node's energy flow output, V denotes the carbon potential energy of the node.

$$\tau = \frac{C_{clean\ use}}{C_{use}} \quad (6)$$

τ is the clean energy carbon utilization rate, which is accounted for in terms of carbon emissions. The application is able to visually characterize the clean energy consumption of each node in the constructed carbon network scenario.

$$\xi = 1 - \frac{C_{loss}}{C} \quad (7)$$

ξ is the energy carbon utilization rate, which is used in carbon networks to assess the carbon emission potential of a single type of energy source versus the carbon emission impact of access losses on the overall energy system.

2.2. Basic principle

Based on the definition of carbon intensity in the literature Méndez et al. (2021), the energy-carbon flow node network modeling is carried out establish on the energy merging principle, energy dispatch principle, the carbon flow principle, and the conservation principle.

Energy merging principle:

There are different types of energy sources for sinking at the i-node. Where ϕ is the energy flow sinking on i-node, the set K characterizes the energy type, and the set Ω characterizes the magnitude of the sink energy flow.

$$\phi_i = \sum_{n \in K, m \in \Omega} (\phi_n * m_n) (K = [E, G, H], \Omega = R^+) \quad (8)$$

Energy dispatch principle:

Take i-node as an example, which injects different types of energy flow to nodes with different types of demands. Where 1 set represents different injected nodes. $\phi_i = \sum_{l \in \Omega} \sum_{n \in K, m \in \Omega} (\phi_{n,l} * m_{n,l}) (K = [E, G, H], \Omega = R^+) \quad (9)$

Carbon flow principle:

The carbon flow principle is simplified compared to the energy flow

scenario due to the singularity of its own flowing material. ρ_l is the carbon emission coefficient per unit of energy flow, and m_l is the size of the tributary energy flow.

$$C_i = \sum_{l, m \in \Omega} (\rho_l * m_l) (\Omega = R^+) \quad (10)$$

The conservation principle:

Both energy and carbon flow obey the principle of conservation in network, and energy flow and carbon emissions do not arise out of thin air or disappear for no reason.

$$\phi_i = \sum_{m \in \Omega} (\phi_m + \phi_{m, loss}) (\Omega = R^+) \quad (11)$$

$$C_i = \sum_{m \in \Omega} (C_m + C_{m, loss}) (\Omega = R^+) \quad (12)$$

3. Energy-carbon network modeling

Carbon flow under the IES follows the flow of energy, and there are multiple energy sources and different sources of energy supply for different users. Each type of energy carries a specific carbon emission profile, which converges and accumulates along transmission pathways in the energy network. These flows eventually converge at system nodes and aggregating at the user side. Clarifying the relationships and modelling the associated carbon networks is the basis for accurate carbon traceability.

3.1. Energy network

3.1.1. Electric grid

The grid side model is as shown below (Cheng et al., 2019):

$$P_{Gi} - P_{Li} = U_i \sum U_j (R_{ij} \cos \theta_{ij} + B_{ij} \sin \theta_{ij}) \quad (13)$$

$$Q_{Gi} - Q_{Li} = U_i \sum U_j (R_{ij} \cos \theta_{ij} - B_{ij} \sin \theta_{ij}) \quad (14)$$

Eq. (13) - Eq. (14) show the generic energy flow calculation model of the grid side. P_{Gi} is the active generation power at node i, P_{Li} is the active load power at node i; Q_{Gi} is the reactive generation power at node i, Q_{Li} is the reactive load power at node i, where U_j is the voltage at node j, R and B are the real and imaginary parts of the node admittance matrix, respectively, θ_{ij} is the voltage phase difference between i and j.

The size of the photovoltaic (PV) capacity is highly dependent on the angle of the installation and the local climatic conditions (Zhu et al., 2023; Talihati et al., 2025).

3.1.2. Coupling model

The combination of the combined heat and power unit(CHP) and a heat pump system creates a coupling of electrical and thermal energy, which together form a thermoelectric coupling model. Construction of a thermoelectric coupling model based on a conventional model (Zhu et al., 2020).

$$\eta_{e-h} = \frac{E_h}{E_e} \quad (15)$$

$$\eta_{h-e} = \frac{E_e}{E_h} \quad (16)$$

$$P_{e-h} = P_e * \eta_{e-h} \quad (17)$$

$$P_{h-e} = P_h * \eta_{h-e} \quad (18)$$

$$P_h = 2.58 * P_e \quad (19)$$

As defined in Eq. (15) - Eq. (19) above, it is a thermo-electric coupling model, in which η_{e-h} is the conversion efficiency of electricity to heat,

and η_{h-e} is the efficiency of converting heat to electricity; E_h is the energy of heat, and E_e is the energy of electricity; P_{e-h} is the power of converting the energy of electricity to heat, and P_{h-e} is the energy conversion of converting the energy of heat to electricity; P_e is the power of electric energy, and P_h is the power of thermal energy power.

In Fig. 3, the model diagram of thermoelectric coupling is defined, in which node 3 and node 4 are thermal energy nodes, which are followed by heat pumps, and node 1 and node 2 are electrical energy nodes. The thermal energy and electrical energy are converted into energy flow through CHP.

3.1.3. Natural gas - heat grid

Thermal energy models are mainly categorized into electric and gas-thermal models (Li et al., 2023).

$$H_{GB} = \frac{V_{GB}\eta\beta}{\Delta t} \quad (20)$$

The thermal power output from the gas boiler is defined in Eq. (20). Where V_{GB} is the inlet gas volume at moment t in m^3 , η is the thermal efficiency of the gas boiler, β is the calorific value of natural gas.

The gas boilers used in the building are operated in an automatic mode, which starts heating when the water temperature falls below the set value and heats the water to the set temperature.

$$Q = c^*m^*(t_s - t_0) \quad (21)$$

Eq. (21) is the equation for the heat absorption of water, c is the specific heat capacity of water, m is the mass of water, t_s is the outlet water temperature t_0 is the inlet water temperature, and the gas usage can also be calculated based on the actual water demand.

$$H_{loss} = c^*m^*(t_{in} - t_{out}) \quad (22)$$

$$t_{out} = (t_{in} - t_{air}) * e^{-\frac{\xi^*L}{c^*m}} + t_{air} \quad (23)$$

The above equation represents the heat loss of the thermal network, where t_{air} is the air temperature, ξ is the heat transfer coefficient of the pipe, and L is the length of the pipe.

$$H_{EB} = P\eta t \quad (24)$$

Eq. (24) is the thermal power of the electric boiler, P is the boiler power, η is the conversion efficiency, and t is the operating time. Heating at a fixed water temperature according to the time of use in the calculation process.

3.2. Energy-carbon network modeling and energy-carbon mapping

Energy flow coupling is in the transmission process of energy flow of the existence of its own carbon characteristics, in a single energy source does not exist in the coupling relationship, but a single mapping

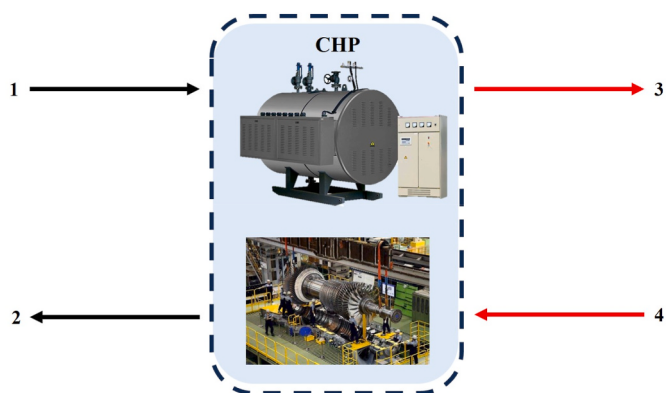


Fig. 3. Thermoelectric coupling model.

relationship, if the energy scenario complexity of the coupling will then be reflected in the transmission process. In order to better sort out this coupling process, a carbon network model is constructed for analysis, which can show the relationship between energy and carbon emissions and the carbon properties of energy well enough.

3.2.1. Network model

Carbon network contains transmission channels and network nodes, each node is connected through the physical energy network, using energy as a carrier for the transfer of carbon flow. The pathways are the transmission routes for carbon flow, while the nodes are responsible for the generation and consumption of carbon flow.

The key nodes of the network are categorized by the node energy supply relationship and contain two major categories: source nodes and energy-using nodes. As shown in Fig. 4 where the upper part is the dynamic carbon network model, in which the nodes have different functions, and the lower part is its functional breakdown and all the functional combinations of the nodes.

As demonstrated in Fig. 4, the carbon flow network model has been derived from a range of energy network models. The channel is transformed from the energy model. Distinguishing between different energy sources at the node level and combining different functions results in the transformation of multiple energy flows along the path into a single carbon flow.

The source nodes are divided into traditional energy Node 1 and the RE Node 4 based on the type of energy; where Node 2 is an energy-using node; special Node 3 has the special function of energy conversion, which represents CHP node in this paper, and it can carry out heat-electricity energy conversion. According to the specific function combination of nodes can be divided into single function nodes, dual function nodes, and multi-function nodes. Through the combination of different nodes and the connecting pathways between the nodes, the corresponding energy-carbon flow network is constructed. Each node can be assigned a node type combination and a node type value according to the actual situation.

3.2.2. Fusion of LCA and carbon emission factors

The carbon factor method establishes a correlation between real-time energy consumption and operational emissions through the utilization of standardized emission coefficients, thereby ensuring temporal precision for short-term dynamic tracking. Conversely, the Life Cycle Assessment (LCA) method quantifies the accumulated embedded emissions associated with energy infrastructure over its full life cycle. This includes the manufacturing, transportation, installation, operation, and decommissioning stages. From an energy flow perspective, these two approaches can be seamlessly integrated by projecting both types of emissions onto the same energy carrier paths. This objective is realized through the establishment of a carbon flow network in which embedded emissions (as determined by the LCA) and operational emissions (as captured by carbon factors) are collectively mapped using node carbon potential and channel carbon resistance. This approach facilitates a coherent spatiotemporal representation of carbon flows.

In order to elucidate the discrepancies and complementarity between the aforementioned methodologies, Table 2 provides a synopsis of their respective characteristics in terms of temporal scale, applicable granularity, emission source scope, data dependence, and adaptability to real-time scenarios. The LCA method is well-suited to long-term infrastructure planning and device-level assessment, with a focus on cumulative carbon impact and high data intensity. Conversely, the carbon factor method is oriented towards real-time system monitoring, with low data overhead and high temporal resolution. The proposed dynamic carbon network model integrates these methods by aligning both emission sources along energy flow paths, allowing their joint expression in the form of carbon potentials and resistances. This fusion enables the model to simultaneously capture historical emission baselines and real-time carbon dynamics, thereby enhancing its practical value in both

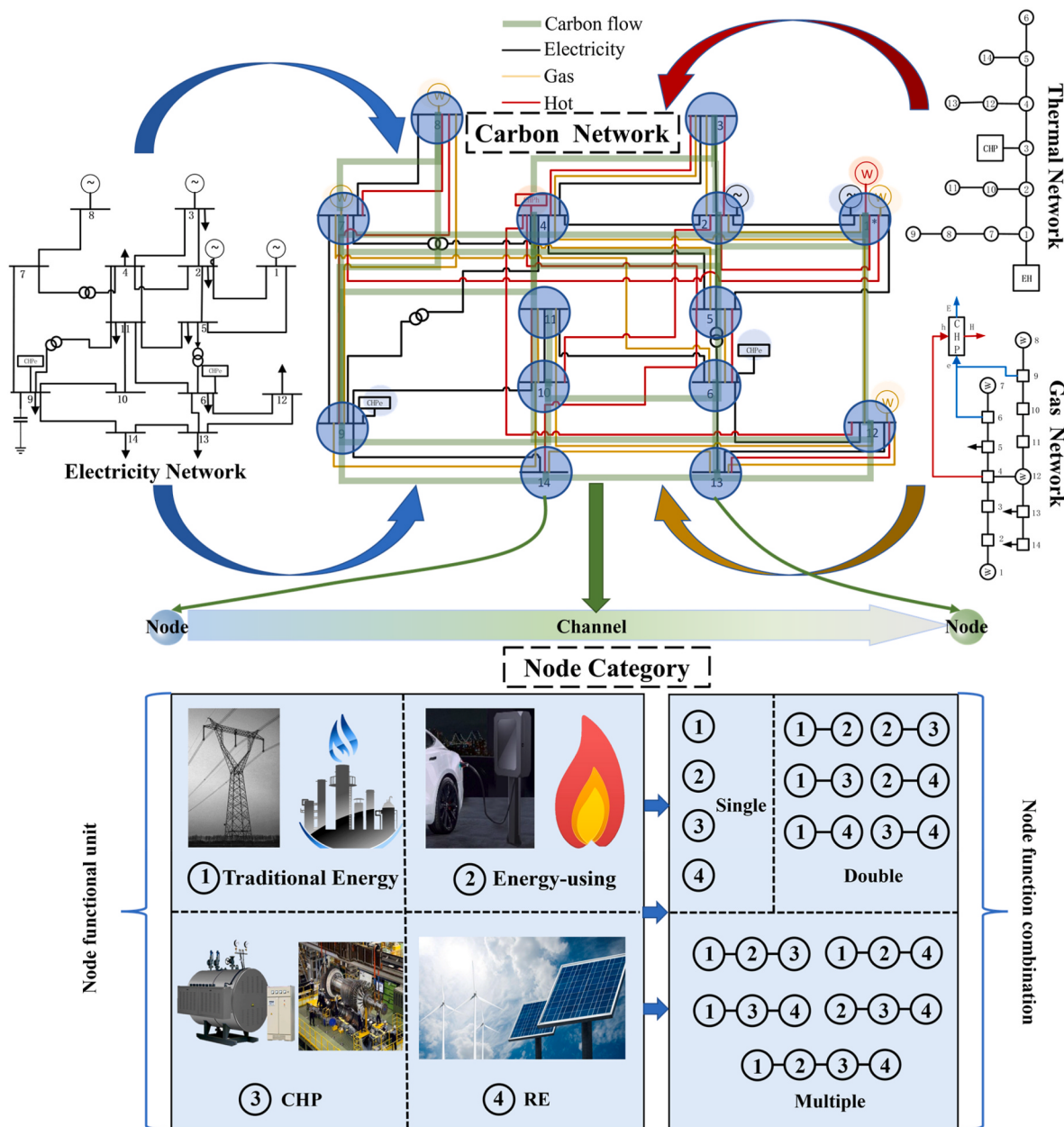


Fig. 4. Carbon flow propagate network.

Table 2

Comparative analysis of carbon emission verification methodologies.

	Carbon factor	LCA	Fusion method (This work)
Scope Boundary	Carbon emission only Direct carbon emission and partial indirect carbon emission	Covers a wide range of environmental impacts Cover the entire life cycle	Carbon emission only Direct carbon emission and the entire life carbon emission of energy equipment
Data requirement Complexity	Energy data and emission factors Simple	Throughout the life cycle Complexity	Energy data and Detailed data throughout the life cycle Complexity in data preparation period, simple in calculation
Time dimension Application scenario	Rely on data at a specific point in time Rapid carbon emission calculation and comparison	Consider changes in technology and time Product manufacturing design and comprehensive assessment	Rely on data at a specific point in time Rapid carbon emission calculation and comparison

planning and operational optimization scenarios.

As demonstrated in Fig. 5, for the overall fusion architecture, in conjunction with the characteristics of carbon emission factors and the LCA method, it is imperative to convert carbon emission per unit energy of the LCA method. The calculation of the carbon flow is then performed

and converted under the network architecture, thus resulting in the construction of the carbon emission network model of the entire integrated energy system.

The LCA method can be used as a basis to obtain the total historical carbon emissions, based on that the calculation of historical carbon

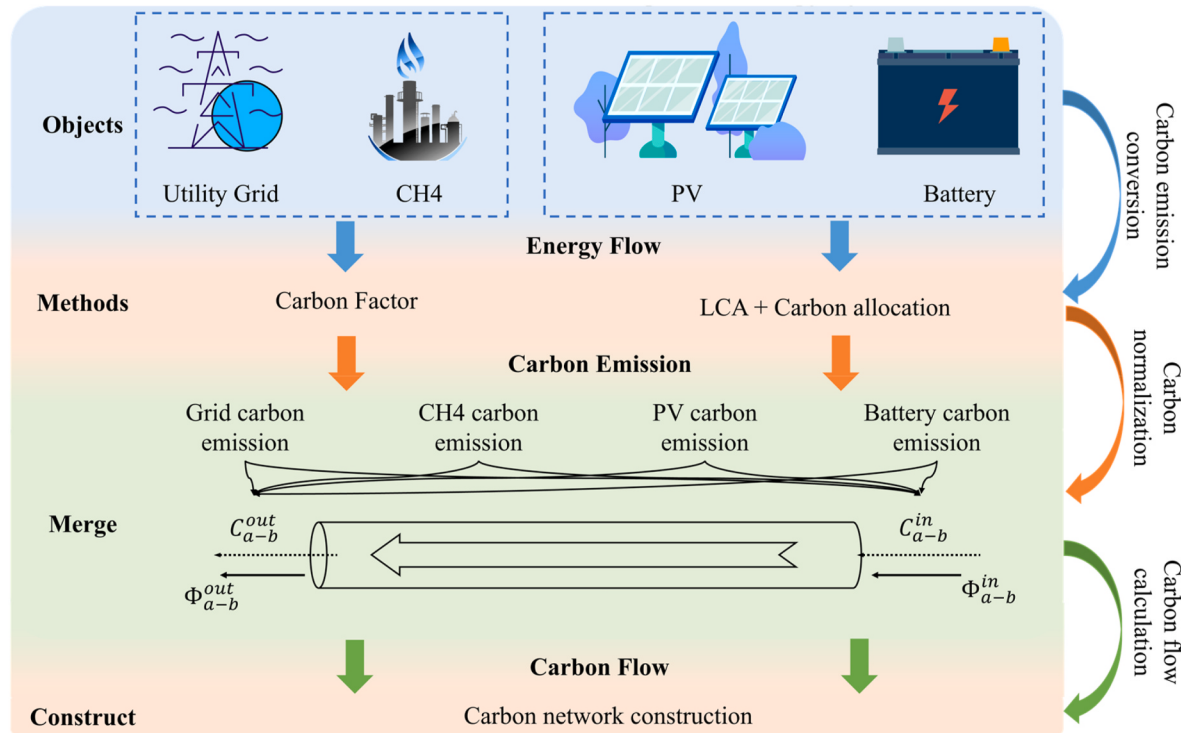


Fig. 5. Carbon emission fusion architecture.

emissions per unit of energy can be carried out:

$$\rho_{history} = \frac{C_{LCA}}{\sum_{y=1,2,3,\dots,N} \Phi_y} \quad (25)$$

Where $\rho_{history}$ is the historical carbon intensity of a specific energy unit, C_{LCA} is the total historical carbon emissions, and Φ_y is the annual energy production potential. The annual capacity potential due to the loss of equipment itself will be presented on an annual basis, in the case of photovoltaic power generation of the annual attenuation rate. The aging caused by the age of the equipment is force majeure, and the total amount of carbon emissions is averaged to increase the reasonableness of the carbon emissions calculation in the subsequent carbon emissions allocation.

To ensure consistency between the LCA-derived embedded emissions and the real-time carbon factor method, several coordination measures have been implemented in the model.

First, in terms of data structure, LCA data are typically equipment-oriented and report cumulative emissions per unit of capacity (e.g., kg CO₂/kWp), while carbon factor data are derived from regulatory or statistical sources and reflect average operational emissions per unit of energy consumed (e.g., kg CO₂/kWh). To reconcile these formats, all carbon data are converted to a unified energy-based reference frame (MWh), allowing for consistent comparison and integration across both emission types.

Second, temporal and regional consistency is maintained by aligning all LCA entries and carbon factor data to the same statistical year and geographical region. This ensures coherence in emission calculations and avoids potential biases introduced by temporal mismatches or spatial heterogeneity in energy system structures and carbon intensity baselines.

Third, for critical energy devices such as photovoltaic panels and combined heat and power (CHP) units, a cross-validation process is applied. Embedded emission factors from LCA databases are compared with operational emission estimates derived from energy use trajectories and standard carbon factors. Where deviations are observed,

adjustments are made to ensure internal consistency and prevent duplication or omission of emission contributions.

The following example illustrates a PV system. Initially, the PV system must undergo verification for carbon flow. Subsequently, its decay factor is to be considered in conjunction with the total energy production throughout the entire life cycle. Finally, mapping the carbon emission to the unit energy as illustrated in Fig. 6.

The general data base is used to analyze the PV system (Wu et al., 2015). The analysis indicates that the total carbon emissions of a 1MWp polycrystalline silicon solar photovoltaic system are approximately 1477t, with carbon dioxide emissions resulting from overall electricity consumption accounting for around 57.1 % of the total emissions, and metallurgical production contributing approximately 8.1 %.

The analysis of PV generation and its attenuation characteristics is instrumental in facilitating the comprehensive evaluation of total power generation throughout the entire life cycle. This analysis is conducted under the assumption of a fixed inclination angle of 30° north latitude and 15° south orientation.

$$C_{cur} = \rho_{cur} * \Phi_{cur} \quad (26)$$

The above equation is used to calculate the current carbon emissions, where ρ_{cur} is the current carbon emission potential per unit of energy, which depends on the link loss and source node carbon emission potential.

$$\rho_{le} = \left(\sum_{n \in N} R_c^{n-i} * P_i + \sum_{n \in S} R_c^n * P_n \right) / \sum_{n \in S} P_n \quad (27)$$

Where R_c is the carbon resistance unit t/kWh, which is used to represent the equalized carbon emissions versus the energy unit carbon emissions. Where N is the collection of nodes through which energy flow, S is the collection of energy supply nodes, P_i is the node energy flow, and P_n is the source node energy flow. Finally, real-time dynamic network carbon emission data is obtained.

$$\rho_{CHP_cur} = \rho_{G_cur} * \eta_{CHP} \quad (28)$$

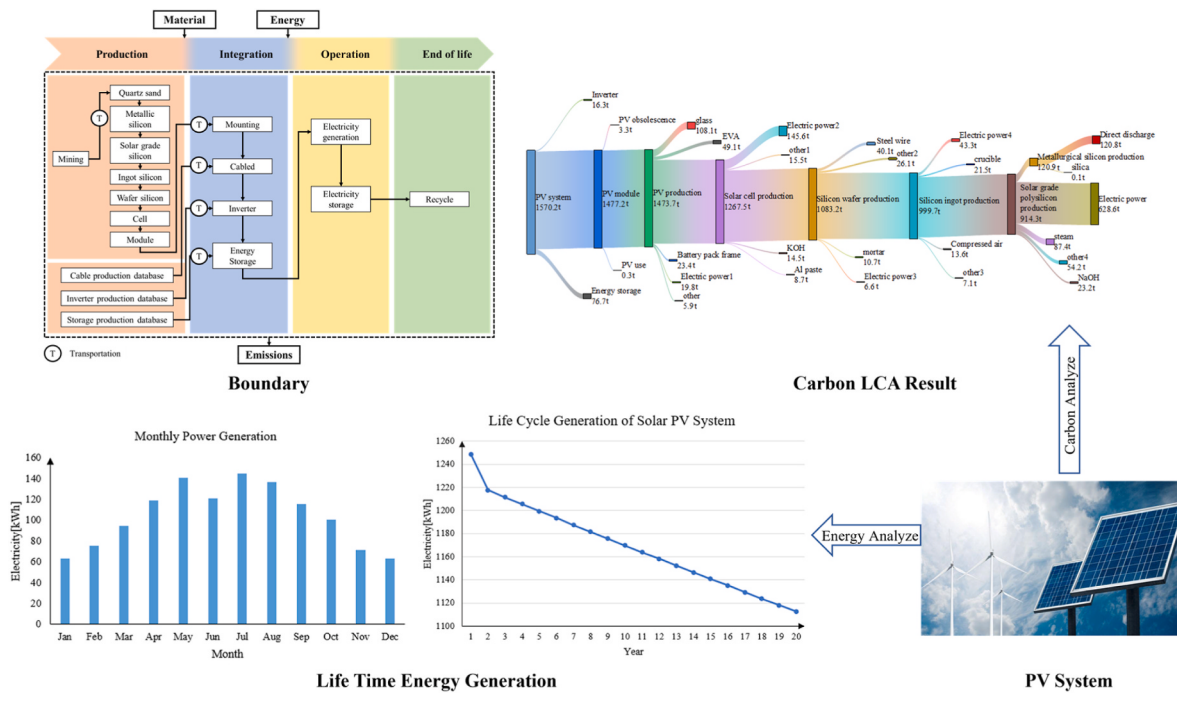


Fig. 6. Carbon flow analyze in PV system.

$$\rho_{CHP_cur} = \rho_{CHP_E_cur} + \rho_{CHP_H_cur} \quad (29)$$

The heat and power production of CHP is accounted for according to the efficiency of its machinery, and the final result is obtained by aggregating the basic CHP expression with the current carbon emissions of the gas as a benchmark.

Table 3 shows the calculation of historical and current carbon emissions for the key nodes of the network system (Xie et al., 2015; Rossi et al., 2023; Forniés et al., 2021; Notarnicola et al., 2017; Miller et al., 2019; Kannan et al., 2006). Since PV is recognized as a the RE source during its use, there are no current carbon emissions.

3.2.3. Energy-carbon mapping analysis and calculation

Carbon emissions in the pathway are propagated by the energy in the channel as a carrier, in which the loss of energy generated by the loss of carbon emissions do not lose with the loss of energy, the corresponding channel due to the loss of energy in its corresponding current carbon emissions factor will also increase. Literature Hiremath et al. (2015) describes the construction of carbon networks, but failed to form the IES applicable model for more energy scenarios. The following equation shows the input and output of carbon emissions in a single-single node:

$$C_{a-b}^{in} = \Phi_{a-b}^{in} * R_{a-b}^{in} \quad (30)$$

$$C_{a-b}^{out} = \Phi_{a-b}^{out} * R_{a-b}^{out} \quad (31)$$

Table 3

Calculation results of carbon emissions at key nodes.

Node type	Historical carbon emissions(kg/MWh)	Current carbon emissions (kg/MWh)	ε
Thermal Power Generation	5.2	581	0.89 %
PV Power Generation	50.2	0	100 %
Gas Source	22.3	198	10.12 %
CHP Power Generation	12.3	246	4.76 %
CHP Heat Generation	31.8	246	11.45 %

$$\Phi_{a-b}^{in} = \Phi_{a-b}^{out} + \Phi_{a-b}^{loss} \quad (32)$$

As illustrated in **Table 4**, the 'single-single' scenario is a relatively straightforward example. The input and output flux is characterized by the presence of carbon flow C, which accompanies the input energy flow

Table 4

Calculation method of IES carbon flow model.

Scenario	Implication	Formula
Single-Single	C_{a-b}^{out} : a,b:Node Φ_{a-b}^{loss} :Energy loss from a to b	(30) (31) (32)
Multi-Multi	C_{a-b}^{use} :Carbon flow from a to b Φ_a^{emit} :Energy flow from a V_a :Carbon potential energy C_{i-a}^{in} :Carbon flow from i to a Φ_{i-a}^{in} :Energy flow from i to a R_{i-a}^{in} :Carbon resistance between i, a Φ_m^{in} :Energy flow from m $E_{l_i-m_in}$:Electricity identification $G_{l_i-m_in}$:Gas identification $H_{l_i-m_in}$:Heat identification Φ_{i-a}^{use} :Use of energy at node m $\Phi_{m-n_i}^{out}$:Transfer of energy from m to n	(33) (34) (35)
Channel	$R_{l_i-m}^{in}$:Carbon flow flowing into node m $R_{l_i-m}^{in}$:Carbon resistance of path l into m V_m :Carbon potential on node m C_m^{emit} :Carbon flow flowing from node m	(39) (40)
Node	C_m^{in} :Carbon flow flowing into node m $R_{l_i-m}^{in}$:Carbon resistance of path l into m V_m :Carbon potential on node m C_m^{emit} :Carbon flow flowing from node m	(39) (40)

φ . Additionally, the energy expended on transmission engenders a concomitant carbon flux, which can be designated as the input side subsequently shared by the user.

The situation of multi-multi nodes is more common:

$$C_{i-a}^{in} + C_{j-a}^{in} + C_{k-a}^{in} = \varphi_{i-a}^{in} * R_{i-a}^{in} + \varphi_{j-a}^{in} * R_{j-a}^{in} + \varphi_{k-a}^{in} * R_{k-a}^{in} \quad (33)$$

$$C_{a-p}^{in} + C_{a-q}^{in} = \varphi_{a-p}^{in} * R_{a-p}^{in} + \varphi_{a-q}^{in} * R_{a-q}^{in} \quad (34)$$

$$\varphi_a^{emit} = C_a^{use} * V_a \quad (35)$$

V_a is the carbon potential energy on point a in units of t. The expression it describes also conveys the energy-carbon flow mapping. The node carbon potential energy is the relationship between the raw carbon accumulated under the corresponding node in the link system and the corresponding energy flow. The corresponding raw carbon accumulation is shared equally according to the principle of whoever uses it. φ is the node inflow energy in kWh; C is the carbon flow of the pathway in t; and R is the branch energy-carbon flow density in t/kWh.

In the ‘multi-multi’ scenario depicted in Table 4, there exist energy flows transmitted by different branches of i, j, and k, each of which contains a carbon flow C. Concurrently, these energy sources are allocated at node a and will be transmitted downward after utilization by the user at a. Consequently, in addition to the carbon emission potential R that exists on the pathway, it is also necessary to compute the carbon potential V at the node, which can be used to quantify the carbon potential of the downward transmission of the energy flow.

In the actual network model, there are numerous combinations of carbon flow propagation accompanied by energy flows starting from the energy side. The carbon potential energy V of the respective nodes and the carbon emission potential of the pathways are crucial for the calculation of the dynamic propagation.

The energy flow under each pathway contains a single or a plurality of energy sources:

$$\varphi_m^{in} = \begin{bmatrix} \varphi_{l_1-m-E}^{in} & \varphi_{l_1-m-G}^{in} & \varphi_{l_1-m-H}^{in} \\ \vdots & \vdots & \vdots \\ \varphi_{l_i-m-E}^{in} & \varphi_{l_i-m-G}^{in} & \varphi_{l_i-m-H}^{in} \end{bmatrix} \cdot \begin{bmatrix} E_{l_i-m_in} \\ G_{l_i-m_in} \\ H_{l_i-m_in} \end{bmatrix} \quad (36)$$

$$\varphi_m^{use} = [\varphi_E^{use} \quad \varphi_G^{use} \quad \varphi_H^{use}] \cdot \begin{bmatrix} E_{use} \\ G_{use} \\ H_{use} \end{bmatrix} \quad (37)$$

$$\varphi_{m-n_i}^{out} = \varphi_{l_i-m}^{in} - \varphi_{l_i-m}^{loss} - \varphi_m^{use} \quad (38)$$

Where φ_m^{in} is the energy flow into node m from different branches, which contains $\varphi_{l_i-m-E}^{in}$ in electric energy inflow, $\varphi_{l_i-m-G}^{in}$ in gas inflow, and $\varphi_{l_i-m-H}^{in}$ in heat energy inflow; due to the differences in units and so on of the different energy sources, it is necessary to identify them, where $E_{l_i-m_in}$ identifies the type of electricity, $G_{l_i-m_in}$ identifies gas similarly, $H_{l_i-m_in}$ identifies the type of thermal energy. φ_m^{use} is the use of energy at node m, and also identifies the energy type. $\varphi_{m-n_i}^{out}$ is the downward transfer of energy, which can be taken up again in Eq. (32) for another round. The representation of the energy type is also to facilitate the subsequent mapping of the energy flow to the carbon flow conversion process.

From different energy source, the carbon flow relationship under its corresponding pathway can be obtained. Due to the non-uniformity of energy units, the analysis of the overall integrated energy system is complicated. Considering the carbon flow characteristics carried by itself, it can be normalized to carbon as the normalized unit, reducing the two-dimensional analysis to a one-dimensional single analysis. The mapping relationship is introduced through the channel carbon resistance and node carbon potential.

From the above two types of channel carbon emission calculations under the two types of channels can be summarized to generalize the energy-carbon flow mapping relationship:

$$C_m^{in} = \varphi_{l_i-m}^{in} * R_{l_i-m}^{in} \quad (39)$$

$$V_m = \frac{\varphi_{m-n_i}^{out}}{C_m^{in} - C_m^{emit}} \quad (40)$$

The carbon emission factor is subdivided into historical and current carbon emissions based on the whole life cycle carbon emissions under the energy transmission process and the carbon emissions of the energy source itself.

In order to facilitate a more profound comprehension of the IES carbon flow calculation method, examples and explanations are provided in Table 4. It is important to note that the carbon potential energy V of the node and the carbon resistance R of the channel are used to characterize the carbon flow of the node and the channel, respectively. These are jointly used for the calculation of carbon under the overall carbon network.

To address the inherent unit inconsistency across multiple energy carriers—such as electricity measured in kWh, natural gas in m³, and thermal energy in MJ—the model introduces carbon emissions as a unified metric through normalization. Each energy type is converted into its carbon equivalent using standardized carbon emission factors (e.g., kg CO₂/kWh for electricity, kg CO₂/m³ for gas, and kg CO₂/MJ for thermal energy), thus enabling dimensionally consistent comparison and aggregation. This transformation aligns all energy flows within the system into a one-dimensional “carbon domain,” forming the foundation for carbon potential (V) and carbon resistance (R) calculations.

Equations (36)–(40) are thus formulated in carbon terms, ensuring dimensional consistency throughout the energy-carbon mapping network. Specifically, Equations (36) and (37) defines the nodal carbon potential as the ratio of accumulated carbon flow to energy inflow at a node (unit: t/kWh), reflecting the carbon intensity of delivered energy. Equations (38) and (39) represents the carbon resistance of a transmission pathway, defined as the carbon loss per unit of transmitted energy (unit: t/kWh), capturing the emission burden of that path. All variables have been revisited to ensure that their physical units match and that the network propagation of carbon flows preserves both mass conservation and physical interpretability across heterogeneous energy forms.

A detailed summary of emission factors and conversion coefficients used for different energy types has been provided in Table 4, and the normalization logic is visually illustrated in Fig. 4.

3.3. Key assumptions of the model

In order to ensure the reproducibility, accuracy, and applicability of the dynamic carbon network model, this subsection systematically specifies the model’s boundaries, key assumptions, and data granularity.

As outlined in Table 5, the model boundaries are delineated along three dimensions: system boundary, spatial boundary, and temporal boundary. The system boundary encompasses electricity, natural gas, and heating networks, in addition to renewable energy sources and energy conversion equipment, including photovoltaic (PV) systems, gas boilers (GB), and combined heat and power (CHP) units. The spatial boundary encompasses all nodes within the selected Integrated Energy System (IES) region, such as an industrial park or community microgrid. The temporal boundary has been set to real-time dynamic analysis, with data acquisition and carbon factor updates occurring at 1-min intervals.

The model explicitly considers both direct carbon emissions from energy use and life-cycle carbon emissions from key renewable energy equipment. The data collection and update frequencies are specified at a fine granularity in order to capture transient variations. The modelling of equipment efficiencies and operational losses is based on

Table 5
Key assumption in carbon model.

Category	Specific Scope	Description
System Boundary	Energy networks	Includes electricity network, gas network and heating network
	Renewable energy systems	Solar PV generation units connected to the electricity network were considered
	Energy conversion equipment	Including GB, EB, CHP
Temporal Boundary	1-min dynamic update	Energy loads and carbon factors updated every minute
	Carbon Emission Range	Direct emissions
Data and Modeling Granularity	Life-cycle emissions	Energy use and conversion emissions
	Load data acquisition	Emissions from energy equipment during the production process
	Carbon factor update	1-min interval collection
Device performance modeling	Efficiency set by device manuals; eg. PV degradation 2 % (year 1), 0.5 %/year thereafter	1-min interval update
	Equipment loss modeling	Incorporates transmission losses (electric, gas, heat) based on empirical loss curves

manufacturer specifications and empirical data. Specifically, for PV systems, a degradation rate of 2 % is applied in the first year, followed by 0.5 % per year thereafter.

The fundamental assumptions underpinning this approach are outlined in the following section.

4. Carbon flow calculation process

The calculation of carbon energy network is based on the calculation of energy network, in which the carbon flow takes energy as the carrier for the inter-network flow. Therefore, energy flow analysis is a prerequisite for carbon flow modeling.

Carbon flow calculation in the IES carbon flow network is based on

the principles of energy flow calculation, which includes the selection of initial nodes, decoupling of energy sources, and the calculation of carbon resistance and carbon potential energy of each transmission pathway and node. Based on the existing energy network model, IES is abstracted into a carbon node network model, where each node has its actual function, and it is connected through the carbon flow pathway to carry out the carbon flow under the network with energy as the carrier.

The electrical network contains state parameters as voltage magnitude, phase angle, active power, reactive power; the gas network contains pressure, system load; and the thermal network contains branch flow, supply temperature, return temperature, and thermal system load.

The flow chart of carbon flow calculation is shown in Fig. 7, in which the left side is the overall process schematic, and the right side will show the grid trend calculation. The carbon flow calculations for the gas and heat networks are analogous to those for the grid side calculation, which exists in the coupling link in accordance with the CHP calculation process for the decomposition of electric energy and thermal energy, respectively, injected into the corresponding nodes, transformed into the basic energy nodes, the existence of which does not affect the overall calculation process.

The network calculates the dynamic carbon flow values of the respective nodes and branches according to the process, which is dynamically updated with the actual carriers in the network. The distribution of energy, to form a dynamic carbon flow network.

5. Case study

The IEEE14 grid model is employed to analyze the spatiotemporal coupling relationship of energy-carbon flow, and the key index the RE consumption rate τ is analyzed under the evolution scenario. Then, in combination with the actual scenario of an industrial zone in Nanjing, the IES14 node carbon network model was constructed based on the IEEE14 grid model, the Belgian 20-node gas model and the 8-node heat model, and the IES14 node carbon network model was analyzed with reference to the open dataset of residential customer loads (Ausgrid, 2023). The spatial and temporal distribution of carbon flow under its

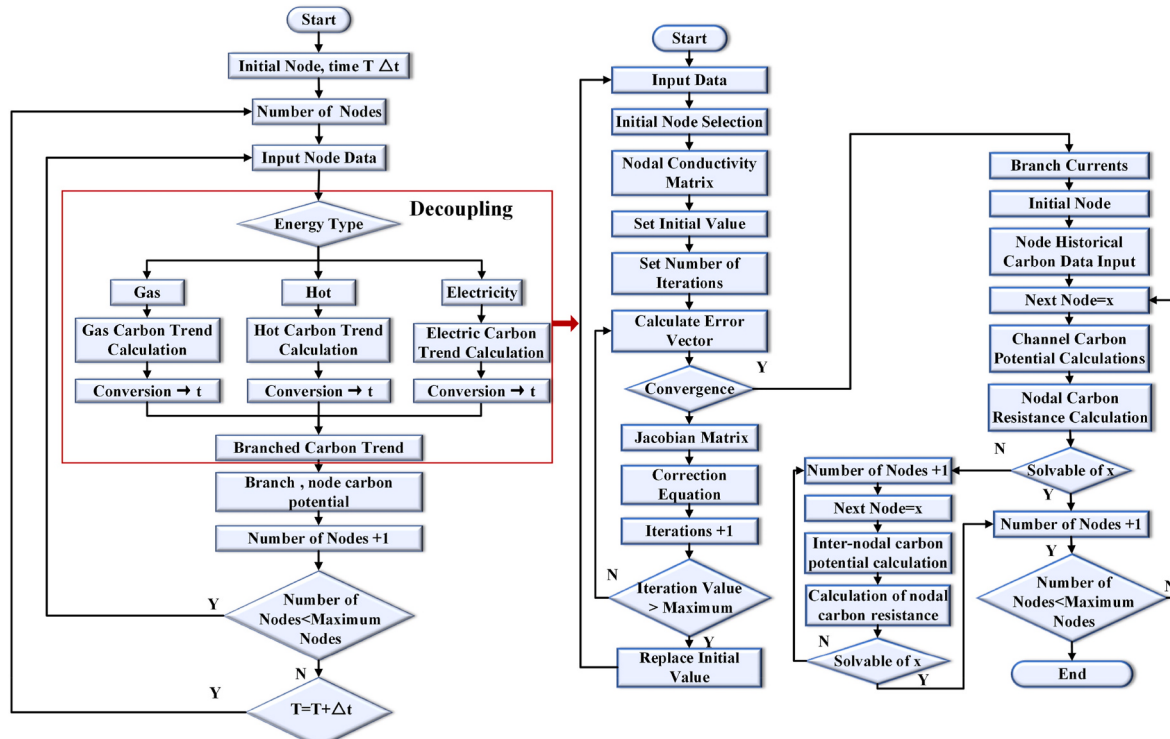


Fig. 7. Flow chart of IES carbon flow calculation.

multi-load scenario is analyzed on the basis of IES network construction, and the key index energy carbon utilization rate ξ is discussed.

5.1. Grid IEEE14 modeling analysis

5.1.1. Energy-carbon flow distribution under the grid

Different definitions have been made for the sources of electrical energy under the conventional node model, defining node 1 as a thermal output node and node 2 as a photovoltaic generation node for the calculations.

In accordance with the type of nodes under the network with conventional network parameters and expanding their node data for historical carbon emissions and current carbon emissions are shown in Table 6. The calculation of historical carbon emissions is derived from the ratio of the product of total carbon emissions and annual electricity generation over the lifetime of the subject. And the current carbon emission corresponds to the carbon emission factor under the corresponding energy source.

The calculation process under the electric energy network is shown in Fig. 8, the calculation is carried out in conjunction with the traditional method of calculating the currents of the electrical energy network to obtain the energy flow situation of the respective branch circuit which is also known as the carbon potential energy value; then the carbon flow is calculated for it.

In order to demonstrate the magnitude of carbon resistance under varying dominant energy access in a more intuitive manner, the carbon resistance of each node is incorporated into the figure for comparison. In Fig. 8, the red color represents the carbon resistance of each node with thermal power, while the blue color represents the carbon resistance of each node with photovoltaic power.

Node 1 exhibits the highest value in the case of a large thermal power output. Upon the dilution of the PV node 2 intervention, there is a notable decline, while the magnitude of the value for each node is also closely related to the selection of the two types of electrical energy output mode. Node 9, for instance, receives a greater amount of photovoltaic power, resulting in a lower carbon resistance value. Since node 8 does not interact with the grid, its corresponding carbon resistance is 0. Conversely, in the scenario with higher PV power output, after the diffusion of thermal power from node 2, the node using more thermal points also causes a higher carbon resistance.

5.1.2. Clean energy carbon utilization rate under photovoltaic evolution τ

In the scenario setting, it is assumed that node 1 is an evolving node, whose energy type is gradually replaced by thermal power to photovoltaic, and eventually becomes a pure photovoltaic under the electric network community. The RE consumption rate τ of each node with its cleaner trend under consumption is analyzed for the state of each node under the IEEE14 network.

As shown in Fig. 9, the nodal carbon dissipation rate analyzes the green power consumption share for each percentage of PV access under the IEEE14 network. Where the red color is the baseline, indicating the percentage of PV access, where the vertical coordinate is the node

Table 6
Node parameters.

Node	Type	Active power (MW)	Load power (MW)	Historical carbon emissions(t/MWh)	Current carbon emissions (t/MWh)
1	Power generation/initial (conventional)	232.84	0	0.0052	0.581
2	Electricity generation (PV)	40	21.7	0.0502	0
3-14	\	\	\	0	0

consumption rate. The green power consumption rate under each PV access ratio at each node is represented by each scatter point in the figure. The PV consumption rate decreases as the PV access ratio of the dominant power node No. 1 increases, and eventually converges with the remaining node ratios.

5.2. IES carbon network system modeling and analysis

The IEEE14 power network is selected as the benchmark for carbon network modeling in microgrid scenarios because the power network contains the node connections of the heat network and is richer in connection types than the heat and gas networks.

5.2.1. IES carbon network construction in microgrid

The electric network is analyzed in more detail, and since most of the sources of heat come from the combustion of petrochemicals, it is singularly merged here into the natural gas network for a unified analysis.

The IEEE14 power network, the Belgian 20-node gas model, and the 8-node thermal model collectively constitute a 14-node carbon network. Due to the large number of nodes in the Belgian gas model, some nodes were merged during model construction, and the final IES14 carbon network is shown in Fig. 10. The type of each node is related to the energy transfer between nodes, where node 1 is the initial node. Red represents thermal energy nodes, black denotes electrical nodes, and yellow indicates natural gas-related nodes.

Each node is functionally divided into residential nodes under the purple circle, in which residential areas are divided into small, medium and large communities according to the community size, and industrial nodes under the gray circle. Electricity is mainly generated by node No. 1 and node No. 2, of which No. 1 has a capacity of 230 MW, No. 2 has a PV capacity of 40MWp, and the whole is equipped with an energy storage of 130 MW, which is mainly used for peak shaving and valley filling.

5.2.2. Spatial and temporal distribution of carbon flow load

The constructed IES14 carbon network model can be more intuitively explored after the transformation of energy flow to carbon flow, and the intrinsic relationship between its carbon flow and energy flow can be derived. A typical winter scenario is selected for analysis because of the large thermal energy demand in winter.

In Fig. 11 illustrates the overall load analysis of the constructed microgrid integrated energy system, in which the node box diagrams, the carbon emission share diagrams of incapable energy consumption, and the thermal analysis diagrams of different energy consumption of each node are constructed from left to right, respectively. From the left diagram, it is obvious to see the difference of carbon emissions of different types of nodes with the size of carbon emissions of different sizes of communities. From the ratio diagram, it can be seen that the proportion of carbon emissions of electric energy is the highest, which is also reflected in the heat diagram, while the heat diagram also illustrates the horizontal comparison of carbon emissions of the same energy source of different nodes, which can be obtained from the difference of electric energy can highlight the scale of carbon emissions of the nodes even more. The difference between the energy use characteristics of the industrial and residential nodes can be clearly seen in the figure, where the residential users have a higher percentage of thermal carbon emissions.

As shown in Fig. 12, it is the carbon emission map of 24h energy consumption within the day, the right panel shows the carbon converted heat map under the IES14 system, and the left side is the carbon emission map of typical nodes. It can be seen that the consumption of thermal energy has a time pattern both higher at night and midday, while the high load of gas and electricity for residential users has a higher time overlap.

The dynamic adjustment capability of the system, enabled by the

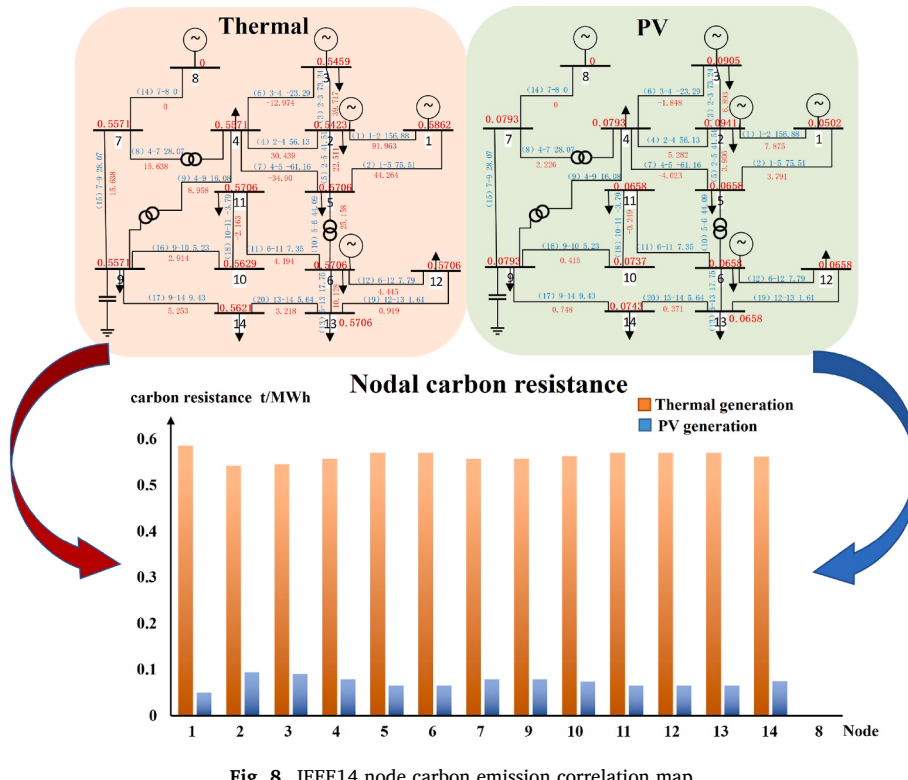


Fig. 8. IEEE14 node carbon emission correlation map.

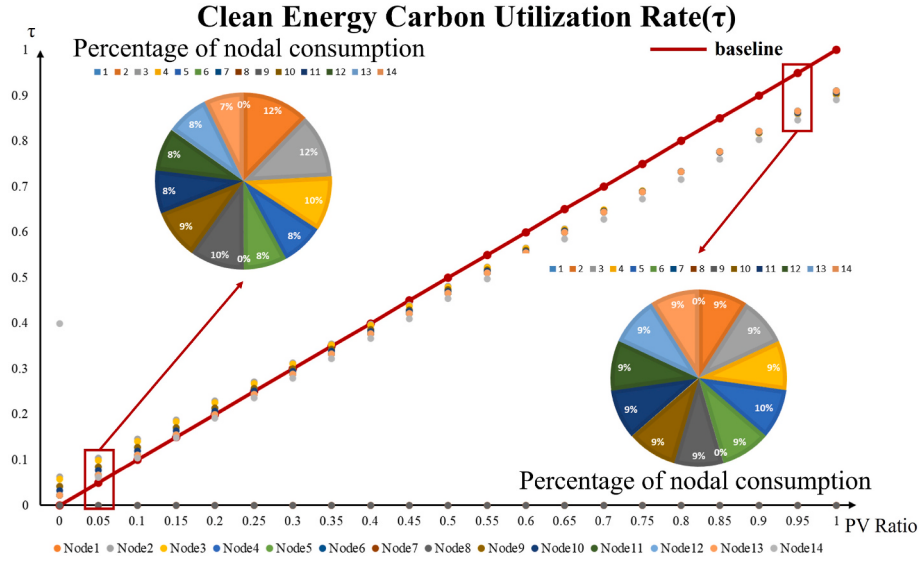


Fig. 9. Nodal carbon dissipation rate.

real-time carbon flow mapping, allows for the smoothing of peak carbon emissions during daytime load surges, thereby supporting more sustainable load balancing strategies.

5.2.3. Consider the energy carbon utilization rate under CHP

IES energy utilization depends mainly on the losses in the process of energy transmission and conversion, and since there are many different types of energy in the integrated energy system, its holistic analysis needs to take into account the types of energy. When the single dimension of carbon is included in the analysis, it is easier to analyze the impact of a single link on the overall IES. It can also be used to determine the potential qualities of the accessed energy sources.

The gas boiler efficiency is carried over at 80 % and the CHP

efficiency is carried over at 90 % in the calculations, where heat production is 2.58 times higher than electricity production.

In Fig. 13 energy carbon utilization can be compared horizontally with the size of the energy utilization of each different node with the same node at different times, such as the left side of the figure illustrates the size of the energy carbon utilization of each energy-consuming node, which can be seen that node 13 has a lower energy utilization rate. The right side of the figure illustrates the IES energy utilization in carbon perspective, where the blue line is the energy utilization rate, which instead shows the opposite trend with the increase of CHP proportion. The reason for this is that as the proportion of CHP access increases, its overall carbon emissions show a decreasing trend, as shown in the figure shows the change curve of total carbon emissions with CHP access. The

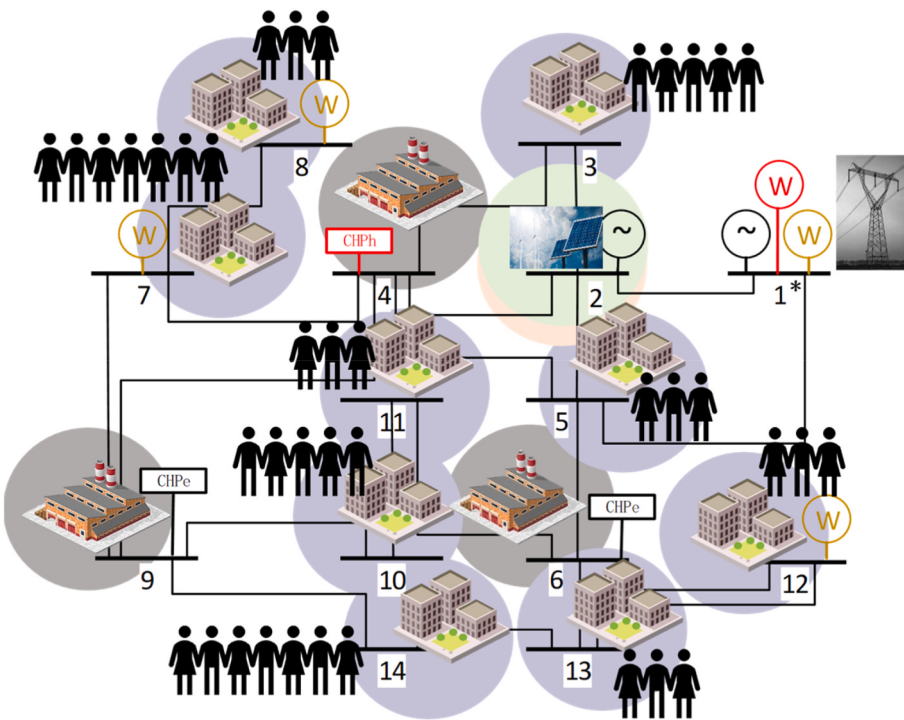


Fig. 10. Functions of nodes.

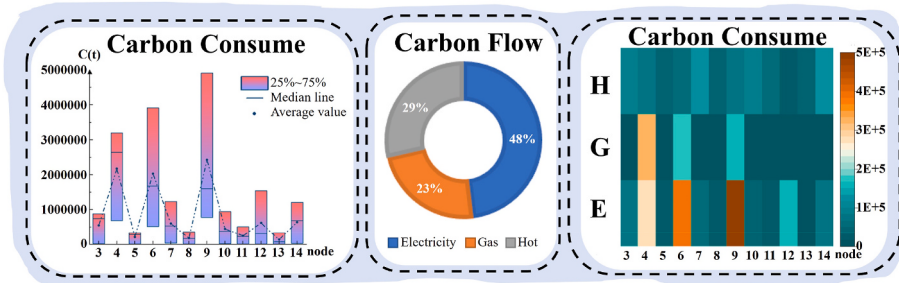


Fig. 11. Carbon emissions analysis in load.

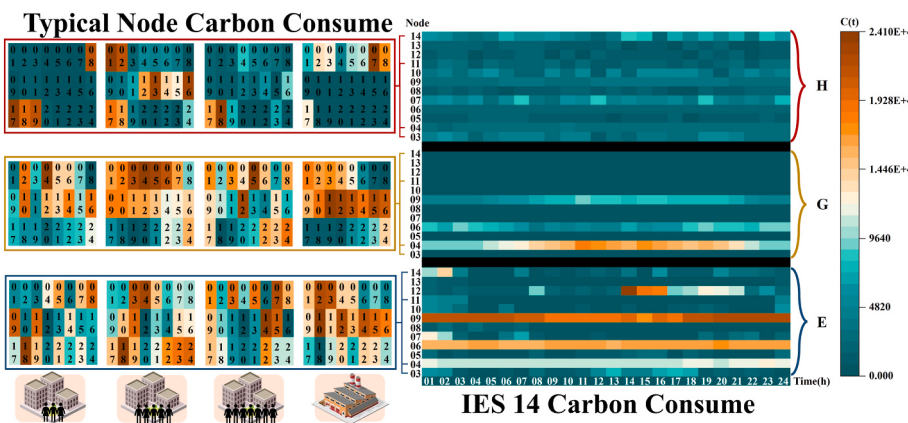


Fig. 12. Intraday load carbon emissions.

results indicate that the reduction in total carbon emissions exceeds the reduction in carbon loss, highlighting the dominant effect of system-level optimization.

As shown in Table 7, The impact of energy carbon utilization ξ on IES

for different types of energy access scenarios is summarized. It can be used to analyze the carbon emission impacts of accessing energy for IES at specific losses.

When the IES system is judged to be a high carbon loss rate system

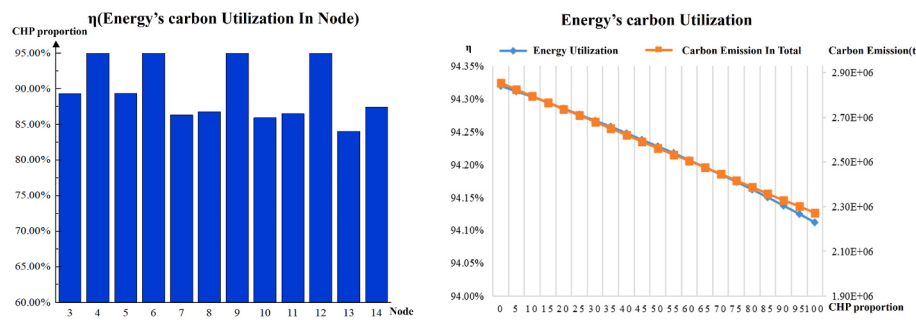


Fig. 13. Energy carbon utilization rate.

Table 7
Relationship between energy carbon utilization and energy access.

	High carbon emission energy	Low- carbon emission energy
ξ increases	Low-loss carbon reduction	Energy-side carbon reduction
ξ decreases	Energy-side carbon increase	High-loss carbon increase

under high utilization energy access, the energy source provides better energy utilization efficiency and also has higher carbon reduction potential, and can be considered as an advanced energy source with a high probability; when the IES system is judged to be a low carbon loss rate system under high utilization energy access, the energy source can provide better carbon reduction capability; when the IES system is judged to be a high carbon loss rate system under low utilization energy access is judged to be a high carbon loss rate system, the energy source can provide better energy utilization; when the IES system is still judged to be a low carbon loss rate system under low utilization energy access, the energy source is not conducive to the carbon emission reduction and energy utilization of the IES system, and can be regarded as a backward energy source.

The use of the indicator ξ can better serve the analysis and energy type optimization of IES. For example, with a 30 % increase in CHP integration, total system carbon emissions were reduced by approximately 9.7 %, while the increase in carbon conversion loss accounted for only 1.8 %, demonstrating that the proposed integration strategy significantly improves overall sustainability performance.

5.2.4. Data errors and sensitivity analyses

Initially, the accuracy of the data was verified, and a typical day was selected for analysis and verification, as illustrated in Fig. 14. This figure is a model error analysis diagram, in which the error between the talent

up data and the model calculated data is marked.

The figure indicates a discrepancy between the collected static carbon emissions data and the model-calculated carbon emissions data, particularly during the midday hours. This discrepancy can be attributed to the fact that the PV carbon emissions verification conducted by the model during the midday hours is also incorporated into the overall carbon emissions. The overall carbon emission verification error for this typical day is 2.73 %.

Assuming an increase in the carbon emission factor of the power node (node 1) from 0.5862 t/MWh to 0.6513 t/MWh, there is a 9.743 % increase in total carbon emissions. Similarly, when the PV carbon emission factor increases from 0.05 t/MWh to 0.056 t/MWh, there is a 0.288 % increase in total carbon emissions. Furthermore, when the power load increases by 10 %, there is a 16.35 % rise in total carbon emissions. Finally, if the PV conversion efficiency were to decrease by 5 %, there would be a 0.12 % rise in total carbon emissions.

As illustrated in Table 8, a comparison of the outcomes from the sensitivity analyses reveals that the electrical energy load demonstrates the highest degree of sensitivity, significantly surpassing the sensitivity

Table 8
Sensitivity analysis results.

Input parameters	Input variation amplitude	Carbon variation amplitude	Data sensitivity
Grid carbon emission	+10 %	+9.743 %	0.97
PV carbon emission	+10 %	+0.288 %	0.03
Electric energy load	+10 %	+16.35 %	3.27
PV conversion rate	-5 %	+0.12 %	0.02

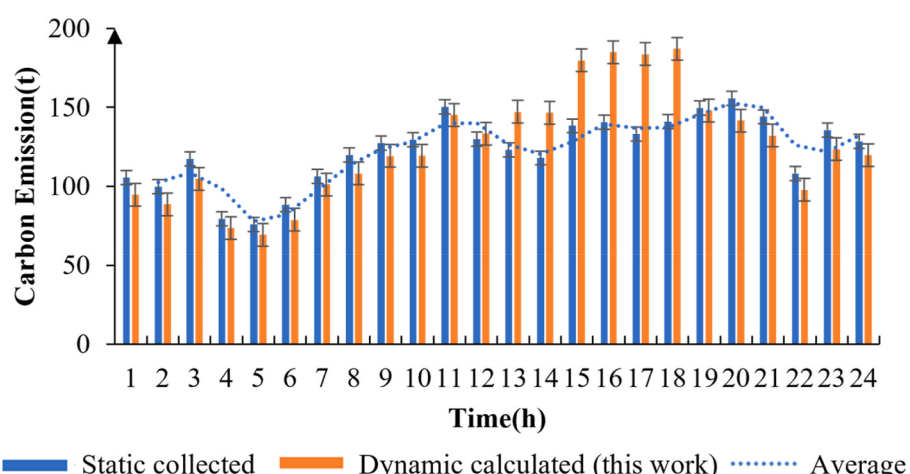


Fig. 14. Typical daily model error analysis.

levels exhibited by the other parameters. Conversely, the sensitivity of the carbon emissions of PV is observed to be comparatively lower.

Moreover, despite a 10 % increase in the electric load, resulting in a 16.35 % increase in carbon emissions, the dynamic carbon network model successfully captured the emission variations with a quantified error margin of less than 3 %, demonstrating its potential to maintain accurate carbon monitoring under fluctuating operational conditions.

6. Conclusion and prospect

6.1. Conclusion

This study introduces the concept of energy-carbon flow mapping and establishes a traceable carbon network model incorporating carbon resistance and carbon potential. Developed through network modeling and the LCA methods, this model aims to dynamically track and trace carbon emissions in IES. Leveraging spatial and temporal scales, the model accurately captures the distributional characteristics of carbon emissions, with a focus on renewable energy consumption rates and carbon utilization. A case study using an IES14 virtual carbon network model for an industrial park in Nanjing demonstrates the model's feasibility and practical applicability. The results indicate that this approach significantly enhances carbon quantification accuracy and enables dynamic carbon traceability within complex energy scenarios. The primary findings are as follows:

1. The application of LCA in carbon flow discounting improves traceability accuracy compared to traditional factor coefficient methods. Specifically, accuracy in accounting rates increased by 0.89 % for electricity, 10.12 % for gas, and 11.45 % for heat production.
2. In an electricity scenario, a carbon network based on the IEEE14 network was established. Precise calculations of carbon potential and transmission resistance at each node clarified the energy-carbon relationship, validating the model's traceability capabilities. Furthermore, renewable energy consumption rates for each node were analyzed from a carbon perspective.
3. Constructed according to carbon network calculation and analysis methods, the model effectively assesses the spatial and temporal distribution of carbon loads in multi-energy scenarios and tracks the carbon emission behavior of users based on their energy consumption patterns.
4. By integrating CHP as an energy substitution within the IES14 network, the model assessed energy carbon utilization across different energy types. Results confirm that this method supports both energy utilization rate assessments and cross-type carbon emission tracking.

This study provides an innovative tool for modeling and analyzing carbon emissions in multi-energy systems, laying a scientific foundation for developing effective low-carbon strategies and optimizing energy structures. By transforming multi-energy data into a one-dimensional carbon network, the approach simplifies multi-energy microgrid analysis, facilitating multi-objective optimization. Furthermore, carbon network analysis integrates both user behavior traceability and comprehensive system-wide insights, contributing to strategic IES design and supporting carbon peak and neutrality goals.

6.2. Prospect

In the application scenarios, the carbon emission accounting model combined with the equipment characteristic model under the selected scenarios can be more suitable for optimal scheduling under the low-carbon goal of energy. The specific implementation process requires the construction of the carbon emission model on the input side of the original energy flow, and at the same time combines with the optimal scheduling algorithms, and gives the strategy with the goal of carbon

emission optimization.

The proposed dynamic carbon network model establishes a physically grounded framework for the implementation of low-carbon energy scheduling by quantitatively linking energy transfer processes with carbon emissions. This is achieved through the definition of two key variables: node carbon potential, which denotes the carbon emission intensity per unit of energy received at a node, and branch carbon resistance, which quantifies the carbon cost per unit of energy transmitted through a given pathway. Together, these parameters constitute a real-time, high-resolution carbon flow distribution over the energy system topology.

This carbon flow information can be directly utilized within optimization and control algorithms to inform dispatch strategies that balance energy demand, operational constraints, and carbon mitigation objectives. Three primary mechanisms for incorporating carbon flow data into scheduling frameworks are proposed:

Objective Function Integration: Carbon flow indicators can be incorporated into the cost function of optimization algorithms. For instance, the system-wide cumulative carbon potential or the total carbon resistance-weighted energy transfer can be minimized alongside conventional objectives such as cost or energy loss. This enables the derivation of scheduling solutions that explicitly prioritize carbon efficiency.

Constraint Formulation: Upper bounds can be imposed on allowable carbon emissions at specific nodes, device-level emission rates, or total system emissions over a given time horizon. These constraints ensure that dispatch decisions remain compliant with carbon reduction targets or regulatory limits.

Feedback-Driven Adaptation: In adaptive or learning-based control paradigms, such as reinforcement learning (RL), the carbon potential and resistance metrics can be encoded within the system state or reward structure. This allows the control agent to iteratively learn dispatch policies that inherently favor low-emission configurations.

The integration of carbon flow metrics into scheduling algorithms such as model predictive control (MPC), multi-objective evolutionary algorithms (MOEAs), or deep reinforcement learning frameworks facilitates the formulation of carbon-aware, dynamic dispatch strategies. In MPC, for example, predicted carbon flow values across the planning horizon can be penalized in the cost function to proactively avoid high-emission states. In MOEAs, trade-offs between energy cost, emission reduction, and system stability can be explicitly explored through Pareto optimization. RL-based methods can leverage carbon flow data to train policies that dynamically respond to load variations and renewable generation uncertainty while minimizing environmental impact.

Overall, the carbon flow network model serves not only as an analytical layer for carbon emission accounting but also as a functional interface between physical energy infrastructure and carbon-aware operational decision-making. By enabling real-time emission traceability and integration into control mechanisms, the proposed framework significantly enhances the capacity of integrated energy systems to achieve adaptive, interpretable, and regulation-compliant low-carbon operations.

Future work will focus on extending the applicability of the proposed framework across diverse regional and operational contexts. The current model validation is based on data from a single industrial park, which, while useful for demonstrating methodological feasibility, inherently reflects specific regional characteristics in energy structure, equipment configuration, and emission profiles. This limitation may restrict the generalizability of the results and reduce the transferability of optimized carbon reduction strategies to other contexts with different boundary conditions.

To address this, the framework will be expanded to incorporate uncertainties in renewable energy generation, such as stochastic photovoltaic output and seasonal wind availability, as well as temporal variability in load demand driven by industrial production cycles or climatic factors. These enhancements will involve the application of

probabilistic modeling techniques and scenario-based simulations to maintain robustness under dynamic operating conditions.

Furthermore, region-specific adaptation will be achieved by integrating localized life cycle inventory datasets, emission coefficients, and energy mix profiles. Such localization will allow the model to reflect spatial heterogeneity in infrastructure, grid carbon intensity, and technological deployment. In addition, incorporating policy-specific parameters—including regional carbon pricing, emission trading schemes, and local decarbonization targets—will enable the model to support compliance-driven optimization.

Through these developments, the framework is expected to evolve into a scalable, adaptive, and policy-aware carbon flow modeling platform, capable of supporting low-carbon energy planning and dispatch strategies that are both technically robust and contextually relevant across multiple regions.

CRediT authorship contribution statement

Bowen Zhang: Writing – Draft and editing, Visualization, Data acquisition. Baligen Talihati: Visualization, Data curation. Hongtao Fan: Proofreading – review & editing. Yaojie Sun: Funding acquisition. Yu Wang: Supervision, Original conceptualization, Writing – review & editing, Funding acquisition.

Declaration of competing interest

The authors declare that they have no known competing financial interests or personal relationships that could have appeared to influence the work reported in this paper.

Acknowledgment

This study was supported by National Natural Science Foundation of China (Grant No. 52407043) and Shanghai Engineering Research Center for Artificial Intelligence in Integrated Energy System (Grant No. 19DZ2252000).

Data availability

Data will be made available on request.

References

- Ausgrid, 2023. <https://www.ausgrid.com.au/Industry/Our-Research/Data-to-share/So-lar-home-electricity-data>. (Accessed 16 May 2023).
- Cheng, Y., Zhang, N., Wang, Y., Yang, J., Kang, C., Xia, Q., 2019a. Modeling carbon emission flow in multiple energy systems. *IEEE Trans. Smart Grid* 10, 3562–3574. <https://doi.org/10.1109/TSG.2018.2830775>.
- Cheng, Y., Zhang, N., Wang, Y., Yang, J., Kang, C., Xia, Q., 2019b. Modeling carbon emission flow in multiple energy systems. *IEEE Trans. Smart Grid* 10, 3562–3574. <https://doi.org/10.1109/TSG.2018.2830775>.
- Cheng, Y., Zhang, N., Wang, Y., Yang, J., Kang, C., Xia, Q., 2019. Modeling carbon emission flow in multiple energy systems. *IEEE Trans. Smart Grid* 10 (4), 3562–3574. <https://doi.org/10.1109/TSG.2018.2830775>.
- Cui, Y., Xu, Y., Huang, T., Wang, Y., Cheng, D., Zhao, Y., 2023. Low-carbon economic dispatch of integrated energy systems that incorporate CCP-P2G and PDR considering dynamic carbon trading price. *J. Clean. Prod.* 423, 138812. <https://doi.org/10.1016/j.jclepro.2023.138812>.
- Deng, Hongwei, 2019. Research on the Calculation Method of Nodal Energy Price for electricity-gas-heat Integrated Energy System Taking into Account the Cost of Carbon Emissions Northeast Power University.
- Forniés, Eduardo, Del Caño, Carlos, Méndez, Laura, Souto, Alejandro, Vázquez, Antonio Pérez, Garraín, Daniel, 2021. UMG silicon for solar PV: from defects detection to PV module degradation. *Sol. Energy* 220, 354–362. Web.
- Hiremath, M., Derendorf, K., Vogt, T., 2015. Comparative life cycle assessment of battery storage systems for stationary applications. *Environ. Sci. Technol.* 49 (8), 4825–4833. <https://doi.org/10.1021/es504572q>.
- Hu, S., Yang, Z., Li, J., Duan, Y., 2021. Economic and environmental analysis of coupling waste-to-power technology to integrated energy system (IES) using a two-layer optimization method. *J. Clean. Prod.* 325, 129240. <https://doi.org/10.1016/j.jclepro.2021.129240>.
- Jiang, T., Deng, H., Bai, L., Zhang, R., Li, X., Chen, H., 2018. Optimal energy flow and nodal energy pricing in carbon emission-embedded integrated energy systems. *CSEEJEPES* 2018.00030.
- J. Power Energy Syst. 4, 179–187. <https://doi.org/10.17775/CSEEJEPES.2018.00030>.
- Kang, Chongqing, Ershun, D.U., Yaowang, L.I., Ning, Z.H.A.N.G., Chen, Qixin, Guo, Hongye, Wang, Peng, 2022. Carbon perspectives on new power systems: scientific issues and research framework. *Grid Technol.* 46 (3), 821–833. <https://doi.org/10.13335/j.1000-3673.pst.2021.2550>.
- Kannan, R., Leong, K.C., Osman, R., Ho, H.K., Tso, C.P., 2006. Life cycle assessment study of solar PV systems: an example of a 2.7 kWp distributed solar PV system in Singapore. *Sol. Energy* 80 (5), 555–563. Web.
- Li, B., Song, Y., Hu, Z., 2013. Carbon flow tracing method for assessment of demand side carbon emissions obligation. *IEEE Trans. Sustain. Energy* 4 (4), 1100–1107.
- Li, J., He, X., Li, W., Zhang, M., Wu, J., 2023. Low-carbon optimal learning scheduling of the power system based on carbon capture system and carbon emission flow theory. *Elec. Power Syst. Res.* 218, 109215. <https://doi.org/10.1016/j.epsr.2023.109215>.
- Méndez, Laura, Forniés, Eduardo, Garraín, Daniel, Vázquez, Antonio Pérez, Souto, Alejandro, Vlasenko, Timur, 2021. Upgraded metallurgical grade silicon and polysilicon for solar electricity production: a comparative life cycle assessment. *Sci. Total Environ.* 789, 147969. Web.
- Meng, F., et al., 2018. Urban carbon flow and structure analysis in a multi-scales economy. *Energy Policy* 121, 553–564. <https://doi.org/10.1016/j.enpol.2018.06.044>.
- Miller, Ian, Gençer, Emre, Vogelbaum, Hilary S., Brown, Patrick R., Torkamani, Sarah, O'Sullivan, Francis M., 2019. Parametric modeling of life cycle greenhouse gas emissions from photovoltaic power. *Appl. Energy* 238 (C), 760–774. Web.
- Notarnicola, B., Tassielli, G., Renzulli, P.A., Monforti, F., 2017. Energy flows and greenhouses gases of EU (european union) national breads using an LCA (life cycle assessment) approach. *J. Clean. Prod.* 140, 455–469. <https://doi.org/10.1016/j.jclepro.2016.05.150>.
- Rossi, F., Zuffi, C., Parisi, M.L., Fiaschi, D., Manfrida, G., 2023. Comparative scenario-based LCA of renewable energy technologies focused on the end-of-life evaluation. *J. Clean. Prod.* 405, 136931. <https://doi.org/10.1016/j.jclepro.2023.136931>.
- Talihati, B., et al., 2024. Energy storage sharing in residential communities with controllable loads for enhanced operational efficiency and profitability. *Appl. Energy* 373, 123880. <https://doi.org/10.1016/j.apenergy.2024.123880>.
- Talihati, B., et al., 2025. Community shared ES-PV system for managing electric vehicle loads via multi-agent reinforcement learning. *Appl. Energy* 380, 125039. <https://doi.org/10.1016/j.apenergy.2024.125039>.
- Tranberg, B., Corradi, O., Lajoie, B., Gibon, T., Staffell, I., Andresen, G.B., 2018. Real-Time Carbon Accounting Method for the European Electricity Markets. <https://doi.org/10.1016/j.esr.2019.100367>.
- Wang, J., et al., 2015. Life cycle assessment (LCA) optimization of solar-assisted hybrid CCHP system. *Appl. Energy* 146, 38–52. <https://doi.org/10.1016/j.apenergy.2015.02.056>.
- Wang, Y., Zeng, B., Guo, Z., Zhang, J., 2016. Multi-energy flow calculationmethod for integrated energy system containing electricity, heat and gas. *Power Syst. Technol.* 40 (10), 2942–2950. <https://doi.org/10.13335/j.1000-3673.pst.2016.10.004>.
- Wang, Y., Qiu, J., Tao, Y., 2022. Optimal power scheduling using data-driven carbon emission flow modelling for carbon intensity control. *IEEE Trans. Power Syst.* 37, 2894–2905. <https://doi.org/10.1109/TPWRS.2021.3126701>.
- Wang, H., Cai, X., Lu, X., Yang, Z., Dong, J., Ma, Y., et al., 2023. A novel load-side settlement mechanism based on carbon emission flow in electricity spot market. *Energy Rep.* 9, 1057–1065. <https://doi.org/10.1016/j.egyr.2023.04.064>.
- Wang, L., Luo, L., Yu, M., Pei, X., 2024. Low-carbon integrated energy system scheduling considering electric vehicle demand response. *J. Clean. Prod.* 480, 144073. <https://doi.org/10.1016/j.jclepro.2024.144073>.
- Wu, P., Xia, B., Wang, X., 2015. The contribution of ISO 14067 to the evolution of global greenhouse gas standards—A review[J/OL]. *Renew. Sustain. Energy Rev.* 47, 142–150. <https://doi.org/10.1016/j.rser.2015.02.055>.
- Xie, Minghui, Ruan, Jiuli, Lu, Bai, Qi, Qiao, Liu, Xiuqiong, Yang, Deren, Yang, Lifei, 2015. Environmental impacts of solar grade polysilicon based on life cycle assessment. *Huan Jing Ke Xue Yan Jiu* 28 (2), 291–296. Web.
- Yan, N., Ma, G., Li, X., Guerrero, J.M., 2023. Low-carbon economic dispatch method for integrated energy system considering seasonal carbon flow dynamic balance. *IEEE Trans. Sustain. Energy* 14, 576–586. <https://doi.org/10.1109/TSTE.2022.3220797>.
- Yang, W., et al., 2023. Mechanism and analytical methods for carbon emission-exergy flow distribution in heat-electricity integrated energy system. *Appl. Energy* 352, 121980. <https://doi.org/10.1016/j.apenergy.2023.121980>.
- Yu, J., Yang, D., Chen, Z., 2021. Multi-energy flow calculation based on energy cell and parallel distributed computation. *Int. J. Electr. Power Energy Syst.* 131, 107147.
- Zhang, Z.-L., Zhang, H.-J., Xie, B., Zhang, X.-T., 2022. Energy scheduling optimization of the integrated energy system with ground source heat pumps. *J. Clean. Prod.* 365, 132758. <https://doi.org/10.1016/j.jclepro.2022.132758>.
- Zhang, H., Sun, W., Li, W., Ma, G., 2022. A carbon flow tracing and carbon accounting method for exploring CO₂ emissions of the iron and steel industry: an integrated material-energy-carbon hub. *Appl. Energy* 309, 118485.
- Zhen, J., Liu, X., Wu, C., Ji, L., Huang, G., 2024. Operation optimization and performance evaluation of photovoltaic-wind-hydrogen-based integrated energy system under carbon trading mechanism and uncertainty for urban communities. *J. Clean. Prod.* 476, 143688. <https://doi.org/10.1016/j.jclepro.2024.143688>.
- Zhu, J., Guo, Y., Mo, X., Xia, Y., Chen, J., Liu, M., 2020. ADP-Based decentralised algorithm for the optimal energy flow of the electricity–natural gas system. *IET Gener., Transm. Distrib.* 14 (8), 1528–1539.
- Zhu, Z., Wang, Y., Yuan, M., Zhang, R., Chen, Y., Lou, G., et al., 2023. Energy saving and carbon reduction schemes for families with the household pv-bes-ev system. *Energy Build.* 288.